PNAS RESEARCH ARTICLE | MICROBIOLOGY

NAD activates olfactory receptor 1386 to regulate type I interferon responses in *Plasmodium yoelii* YM infection

Yu-chih Peng[a,1], Jian Wu[a,1], Xiao He[a,1], Jin Dai[b], Lu Xia[c], Paola Valenzuela-Leon[a], Keyla C. Tumas[a], Brajesh K. Singh[a], Fangzheng Xu[a], Sundar Ganesan[d], Shirin Munir[b], Eric Calvo[a], Ruili Huang[e], Chengyu Liu[f], Carole A. Long[a], and Xin-zhuan Su[a,2]

Edited by L. Sibley, Washington University in St. Louis, St. Louis, MO; received February 27, 2024; accepted April 26, 2024

Olfactory receptors (Olfr) are G protein–coupled receptors that are normally expressed on olfactory sensory neurons to detect volatile chemicals or odorants. Interestingly, many Olfrs are also expressed in diverse tissues and function in cell–cell recognition, migration, and proliferation as well as immune responses and disease processes. Here, we showed that many Olfr genes were expressed in the mouse spleen, linked to *Plasmodium yoelii* genetic loci significantly, and/or had genome-wide patterns of LOD scores (GPLSs) similar to those of host Toll-like receptor genes. Expression of specific Olfr genes such as *Olfr1386* in HEK293T cells significantly increased luciferase signals driven by IFN-β and NF-κB promoters, with elevated levels of phosphorylated TBK1, IRF3, P38, and JNK. Mice without Olfr1386 were generated using the CRISPR/Cas9 method, and the *Olfr1386*$^{-/-}$ mice showed significantly lower IFN-α/β levels and longer survival than wild-type (WT) littermates after infection with *P. yoelii* YM parasites. Inhibition of G protein signaling and P38 activity could affect cyclic AMP-responsive element promoter-driven luciferase signals and IFN-β mRNA levels in HEK293T cells expressing the Olfr1386 gene, respectively. Screening of malaria parasite metabolites identified nicotinamide adenine dinucleotide (NAD) as a potential ligand for Olfr1386, and NAD could stimulate IFN-β responses and phosphorylation of TBK1 and STAT1/2 in RAW264.7 cells. Additionally, parasite RNA (pRNA) could significantly increase *Olfr1386* mRNA levels. This study links multiple Olfrs to host immune response pathways, identifies a candidate ligand for Olfr1386, and demonstrates the important roles of Olfr1386 in regulating type I interferon (IFN-I) responses during malaria parasite infections.

Plasmodium | mouse | G protein–coupled receptor | signaling | immune responses

Significance

Malaria is a parasitic disease that affects hundreds of millions of people and kills over one-half a million people annually. Developing vaccines to prevent malaria requires a good understanding of the mechanisms of disease pathogenesis and host immune responses. Olfactory receptors (Olfr) are normally expressed on olfactory sensory neurons to detect volatile chemicals. Here, we show that various Olfrs are expressed in the mouse spleen in response to malaria parasite infections. We further show that Olfr1386 regulates type I interferon (IFN-I) responses, and deletion of the *Olfr1386* reduces IFN-α/β levels after *Plasmodium yoelii* YM infection. Additionally, we identify nicotinamide adenine dinucleotide as a potential ligand of Olfr1386. This study reveals important functions of Olfrs in malaria parasite infections.

Olfactory receptors (OR or Olfr in mice) belong to the superfamily of G protein–coupled receptors (GPCR) that bind various extracellular ligands such as oligopeptides, metabolites, neurotransmitters, and odorants. These proteins typically have seven alpha-helix transmembrane domains (TMs) with an extracellular N terminus and an intracellular C terminus (1). Structurally, the extracellular regions between TMs 3, 5, and 6 are responsible for ligand binding and recognition, whereas the cytoplasmic region of domains 2 and 3 interact with heterotrimeric G proteins (1, 2). After stimulation by the binding of a specific ligand or odorant, an Olfr is activated, and the α subunit (Gαolf) is released from the heterotrimeric G protein β and γ subunits, leading to adenylate (or adenylyl) cyclase (AC) activation and production of cyclic adenosine monophosphate (cAMP) from ATP (3). The increasing intracellular cAMP concentration opens cyclic nucleotide-gated (CNG) channels and depolarizes cell membranes by the influx of cations (Ca^{2+} & Na^{+}) and efflux of Cl^{-} anion (4–7). Mice deficient in Gαolf, AC, and CNG are anosmic (lacking a sense of smell), suggesting that the G protein-cAMP pathway is essential for olfactory signal transduction (8, 9).

In humans, more than half of the approximately 800 OR genes are pseudogenes (10–12), whereas, in the mouse, fewer than 25% of 1,400 Olfr genes (abbreviated as Olfr for mouse genes) are pseudogenes (13–15). Interestingly, many OR/Olfr genes are expressed in tissues other than the olfactory epithelium, suggesting diverse functions (16, 17). For example, mouse Olfr544 is not only overexpressed in the brain of Alzheimer's disease-like mice (18, 19) but also expressed in the liver and adipose tissue of mice with metabolic syndromes (20, 21). Indeed, Olfr544 can regulate fatty acid metabolism and shift the energy preference by its ligand azelaic acid (20, 21). Some ORs/Olfrs are expressed in the reproductive system, such as the placenta (Olfr56), testis (OR10J1), and sperm (OR2H1/1, OR51E1/2, OR6B2), and may play important roles in sexual reproduction (22, 23). Overexpression of ORs in cancerous cells such as prostate cancer (OR51E1, OR51E2) (24–26), small intestine neuroendocrine carcinoma (OR51E1) (27), hepatocarcinoma (OR1A2) (28), and non–small cell lung cancer

Author contributions: X.-z.S. designed research; Y.-c.P., J.W., X.H., J.D., P.V.-L., K.C.T., B.K.S., F.X., S.G., S.M., and C.L. performed research; Y.-c.P., J.W., X.H., J.D., L.X., P.V.-L., F.X., S.M., E.C., R.H., C.L., and X.-z.S. analyzed data; E.C. supervised research; and C.A.L. and X.-z.S. wrote the paper.

The authors declare no competing interest.

This article is a PNAS Direct Submission.

[1]Y.-c.P., J.W., and X.H. contributed equally to this work.

[2]To whom correspondence may be addressed. Email: xsu@niaid.nih.gov.

This article contains supporting information online at https://www.pnas.org/lookup/suppl/doi:10.1073/pnas.2403796121/-/DCSupplemental.

Published May 29, 2024.

(OR2J3) (29) were also reported. The activation of OR2J3 by helional via ERK can induce cell apoptosis and inhibit cell proliferation in the A549 cell line, while the activation of OR1A2 by (-)-citronellal via P38 MAPK reduces cell proliferation in the Huh7 cell line (29). These observations suggested that ORs are potential therapeutic targets or biomarkers for cancer screening. Additionally, olfactory stem cells on the nasal epithelium could mediate NF-κB-dependent inflammation during neuroregeneration (30, 31). Recently, mouse Olfr78 (OR51E2) was shown to modulate the intestinal response to colitis; significant changes in the expression of the genes involved in infection, immunity, inflammation, and colorectal cancer were detected in Olfr78 knockout (KO) mice (32). Additionally, bitter taste receptors (T2Rs) were found to be associated with infections, including patients infected with SARS-CoV-2 and inflammatory diseases (33–36). Therefore, ORs may function in more than odorant-sensing, playing important roles in various diseases and disorders.

Mosquitoes can sense human sweat via ORs, detecting carbon dioxide, ammonia, L-lactic acid, carboxylic acids, alcohol, and ketones from human hosts (37–39). Interestingly, a mosquito can be attracted by terpenes produced by malaria parasites to facilitate the transmission of malaria (40). However, whether ORs play a role in response to malaria infections in vertebrates is unknown. We previously performed two trans-species expression quantitative trait locus (ts-eQTL) analyses, which use host gene expression levels as phenotypes and parasite polymorphic loci as genotypes in quantitative trait locus analysis, and linked large numbers of mouse genes to *Plasmodium yoelii* parasite genetic loci (41, 42). Interestingly, many *Olfr* genes were significantly linked to parasite loci in host response day 1 postinfection (pi), but not on day 4 pi. It is not surprising that *Olfr* genes responded early in the infection because these receptors could function as sensors of parasite molecules. In this study, we functionally characterized selected mouse *Olfr* genes in response to *P. yoelii* infection and showed that several *Olfr* genes played a role in type I interferon (IFN-I) and NF-κB (nuclear factor kappa-light-chain-enhancer of activated B cells) pathways. We then focused on *Olfr1386* (OR2Y1c in humans) which had genome-wide patterns of LOD (logarithm of the odds) score (GPLS) almost identical to that of Toll-like receptor 3 (TLR3) and showed that Olfr1386 expression could enhance TLR3-mediated responses. Further, expression of Olfr1386 increased the phosphorylation of molecules such as TBK1 and IRF3 leading to enhanced IFN-I responses, and nicotinamide adenine dinucleotide (NAD) was identified as a potential activator of Olfr1386 signaling. This study reveals important functions of Olfrs in regulating host immunity during malaria infections.

Results

Many *Olfr* Genes Significantly Linked to Multiple Parasite Genetic Loci. We previously performed two ts-eQTL analyses using mRNA from mouse spleens infected with progenies of a *P. yoelii* cross (17XNL × N67) on day 1 (24 h) and day 4 pi and linked parasite genetic loci to the expression of over 1,000 host genes (41, 42). In addition to many known immune-related genes, we also noticed many Olfr genes that were significantly linked to parasite genetic loci in the mRNA datasets isolated from the spleens 24 h pi, but not day 4 pi. Reexamining the data from mRNAs of the spleen 24 h pi (42), here we identified 40 Olfr genes that were significantly (LOD score ≥3.0) linked to 54 microsatellites on eight parasite chromosomes (1, 2, 4, 5, 7, 8, 10, and 13) after genome-wide linkage analysis (Fig. 1*A* and Dataset S1). For example, *Olfr134* and *Olfr340* were significantly linked to two microsatellite markers (Py1521 and Py1335) on chromosome 1, respectively (Fig. 1 *A* and *B*), and *Olfr1269* and *Olfr1317* were significantly linked to microsatellite marker Py1341 on chromosome 8 with a similar GPLS (Fig. 1*C*). In contrast, only two *Olfr* genes (*Olfr866* and *Olfr1491*) were significantly linked to two microsatellite markers using mRNA from infected spleens 4 d pi (Dataset S1). Note *Olfr866* was significantly linked to markers on chromosome 2 (Py652 and Py1511) using mRNA from both 24 h and day 4 infected spleens. The results show activation of many *Olfr* genes only during the early stages of infection (24 h), which is consistent with their predicted function acting as receptors in response to malaria parasite infections. Fine mapping and functional characterization of the candidate genetic loci may lead to parasite genes that interact with or regulate the *Olfr* gene expression and signaling.

***Olfr* Genes Clustered with Toll-Like Receptors.** Previously, we also demonstrated that host genes having similar GPLSs were likely to function in the same or related pathways (41). Clustering host genes again identified several *Olfr* genes having GPLSs similar to specific TLRs. For example, *Olfr1386* had a GPLS almost identical to that of *Tlr3* (Fig. 2*A*). Although there were differences in mRNA expression levels of the two genes among the two parental parasites and the progenies from the N67 × 17XNL cross, the parallel trend in mRNA levels for both *Olfr1386* and *Tlr3* in the mice infected with the 24 progenies suggested stimulation of mRNA expression of both genes by a common agent or a shared mechanism, even though the two genes are located on different chromosomes, and there is no detectable homology in the 5'UTRs of the two genes (Fig. 2*B*). Likewise, *Olfr1491* and *Olfr1373* had GPLS patterns similar to that of *Tlr8* (Fig. 2 *C* and *D*). Interestingly, *Olfr1491* was also significantly linked to marker Py1371 on chromosome 13 using mRNA from day 4 infected spleens (Dataset S1). Additionally, *Tlr12* and *Olfr1475* had similar GPLSs, but the mRNA expression patterns among the progeny were quite different between the two genes (Fig. 2 *E* and *F*). Note there are shared LOD peaks between genes such as *Olfr1373, Olfr1386, Olfr1491*, and *Olfr1475* on chromosomes 7 and 8 (Figs. 1 and 2). The similar GPLSs between *Olfr1386* and *Tlr3* genes suggest that the two genes function in related pathways in response to malaria parasite infections.

Expression of Selected *Olfr* Genes Stimulates IFN-β and NF-κB Responses. The observations of similar GPLSs between *Tlr* and *Olfr* genes suggest that some *Olfr* genes may play a role in host innate immune responses, possibly via pathways associated with TLR signaling and IFN-I responses. We transfected HEK293T (human embryonic kidney 293 cells immortalized using SV40 large T antigen) cells with an empty plasmid as control or individual plasmids encoding one of 23 DDK-tagged *Olfr* genes significantly linked to parasite microsatellite markers or with GPLSs similar to those of TLRs. At the same time, plasmids encoding firefly luciferase (FLuc) driven by IFN-β or NF-κB promoter and renilla luciferase (Rluc) driven by β-actin promoter were cotransfected to detect activation of IFN-β or NF-κB promoters. Of the 23 *Olfr* genes analyzed, five (*Olfr279, Olfr1269, Olfr1317, Olfr1373,* and *Olfr1386*) could significantly increase luciferase signals driven by IFN-β and NF-κB promoters when expressed in the HEK293T cells (Fig. 3 *A* and *B*), suggesting potential roles of these *Olfr* genes in regulating host immune responses.

To investigate protein expression and localization in the cells, we transfected HEK293T cells with plasmids (1 μg) encoding DDK-tagged Olfr279, Olfr1269, Olfr1317, Olfr1373, and Olfr1386 and detected the expressed proteins using an anti-DDK antibody. Multiple (smear) protein bands were detected by the

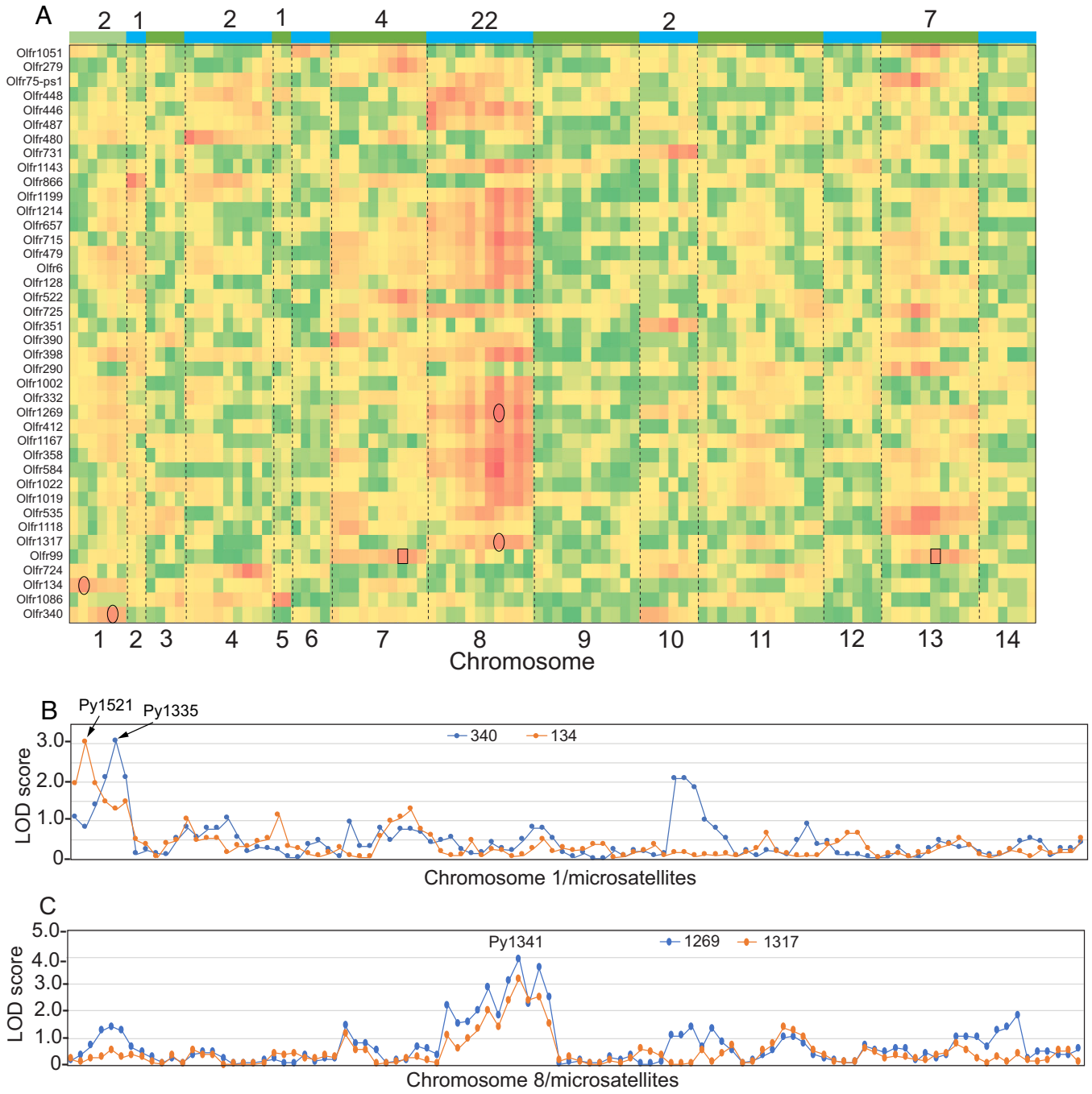

Fig. 1. Linkages of parasite genetic loci to expression levels of *Olfr* genes in the progeny of a *P. yoelii* cross. (*A*) Colorimetric display of genome-wide pattern of LOD scores (GPLSs) for *Olfr* genes significantly (LOD score ≥ 3.0) linked to parasite genetic loci using mRNA from the spleens of the *P. yoelii* 17XNL × N67 cross progenies 24 h postinfection (41). Red, higher LOD score; green, lower LOD score. The total numbers of *Olfr* genes significantly linked to each chromosome are listed on the top of each chromosome. *Olfr* gene IDs are listed on the *Left* side of the figure. Note some *Olfr* genes are significantly linked to two loci (for example, *Olfr*99, highlighted with black rectangles on chromosome 7 and 13). Black circles indicate examples of parasite genetic loci with the highest LOD scores for the corresponding *Olfr* genes. (*B*) Plots of GPLSs for Olfr134 and Olfr340 showing a peak of LOD score ≥ 3.0 on chromosome 1, respectively. The highest LOD peaks and the linked microsatellite markers are as indicated. (*C*) Plots of genome-wide pattern of LOD scores for Olfr1269 and Olfr1317 genes with peaks of LOD score on chromosome 8. Py1341 is a microsatellite marker that is significantly linked to the two *Olfr* genes with the highest LOD scores (≥3.0).

anti-DDK antibody (Fig. 3*C*), which is consistent with the expression characteristics of a membrane protein. We also used anti-Olfr1386 antibodies (Invitrogen, catalog #PA5-70445) to detect the proteins and showed recognition of three Olfr proteins (Olfr1269, Olfr1373, Olfr1386) by the antibodies (Fig. 3*D*). The anti-Olfr1386 antibodies were generated using a peptide at the C terminus of the Olfr1386 (LQPKSSYSES KGKFVALFYT IVTPMLNPLI YTLRNKDVKGALWKVLGRGT, https://MyBioSource.com) with a conserved sequence (TPMLNPLI YTLRN) at TM7 among Olfr1386, Olfr1269, and partially Olfr1373. Immunofluorescence assay (IFA) analysis using anti-DDK monoclonal antibody and anti-Olfr1386 polyclonal antibodies detected signals as puncta in the cytoplasm and at cell peripheral regions, suggesting potential plasma membrane localization (Fig. 3*E* and *SI Appendix*, Fig. S1). No signal was detected by anti-DDK or anti-Olfr1386 antibodies when HEK293 cells were transfected with empty vector without the gene encoding Olfr1386 (*SI Appendix*, Fig. S1).

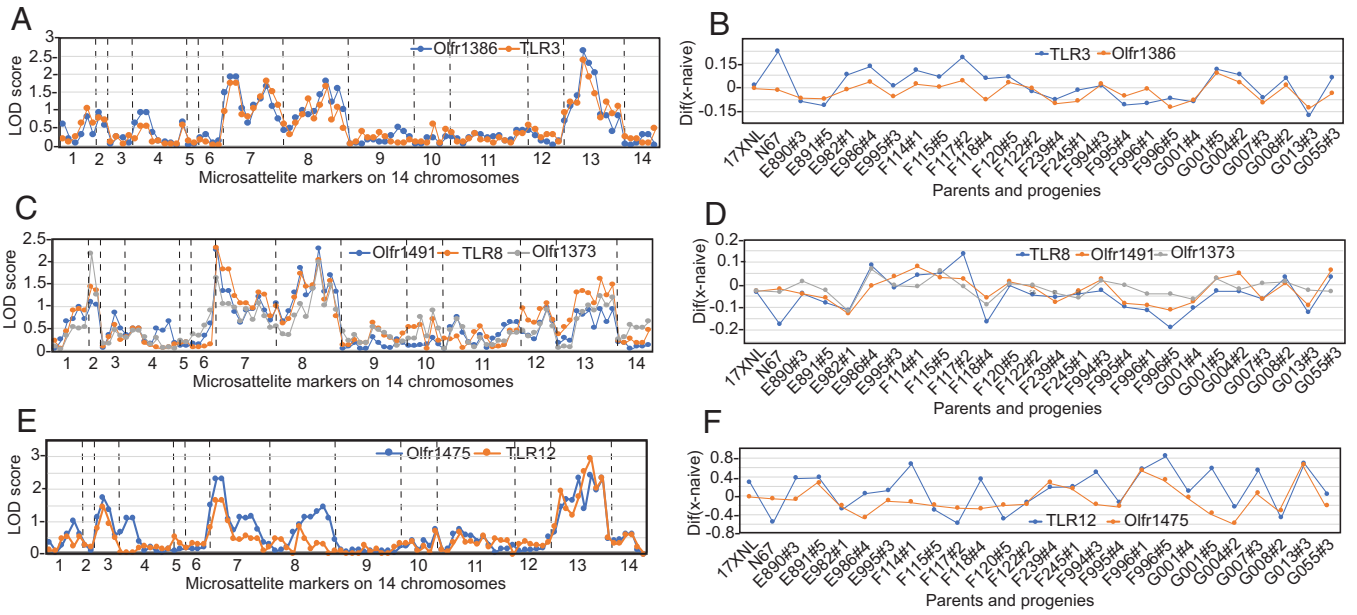

Fig. 2. Clustering genome-wide patterns of LOD scores (GPLSs) and gene expression for selected *Olfr* and TLR genes. (*A* and *B*) Almost identical GPLSs (*A*) but with some differences in mRNA expression patterns (*B*) for Olfr1386 and TLR3 from mice infected with 24 progeny and their parents (17XNL and N67). (*C* and *D*) Similar GPLSs (*C*) and mRNA expression patterns (*D*) for Olfr1373, Olfr1491, and TLR8 genes. (*E* and *F*) Similar GPLS patterns (*E*) between Olfr1475 and TLR12, but quite different mRNA expression patterns (*F*) among the parasites.

We next aligned protein sequences from the 32 Olfrs linked to host responses to malaria parasite infections and performed phylogenetic clustering of the sequences. The protein sequences were downloaded from public databases and were clustered into five major groups, with one group containing Olfr1269 and Olfr1317, and another group containing Olfr1373, Olfr1386, and Olfr279 (*SI Appendix*, Fig. S2*A*). In addition, Olfr1386 and Olfr1373 were clustered together with 75.6% amino acid sequence identity (*SI Appendix*, Fig. S2*B*) and had GPLSs similar to those of TLR3 and TLR8, respectively (Fig. 2 *A* and *C*). Similarly, Olfr1269 and Olfr1317 were also closely related, having 46.0% sequence identity (*SI Appendix*, Fig. S2 *A* and *C*). Interestingly, Olfr1269 and Olfr1317 were significantly linked to marker Py1341 on chromosome 8 (Fig. 1*C*). These results suggest a linkage between the QTL peak or GPLS with specific Olfr amino acid sequences.

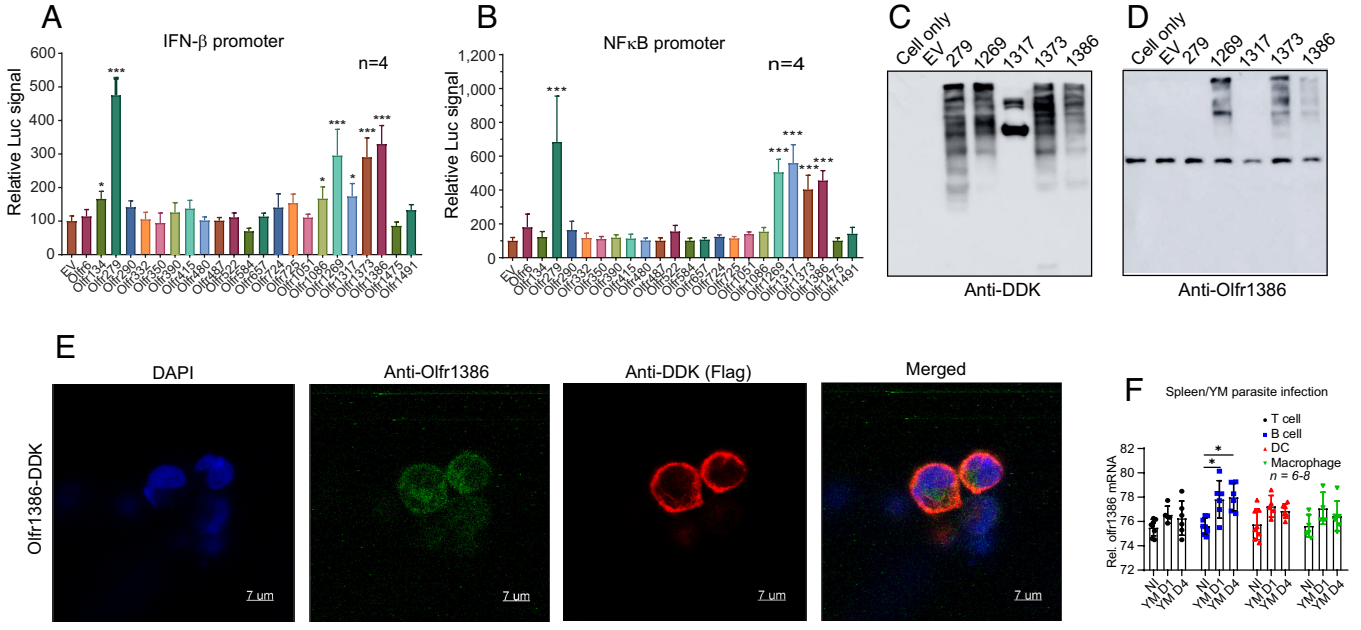

Fig. 3. Olfr expression and the effects on IFN-β and NF-κB responses. HEK293T cells were transfected with plasmids encoding one of the DDK-tagged Olfr genes (90 ng/each) and genes encoding firefly (100 ng) and renilla (10 ng) luciferases as described in *Materials and Methods*. Relative (ratio of FLuc/RLuc) luciferase signals measured 24 h posttransfection are plotted. (*A*) Relative luciferase signals driven by IFN-β promoter after overexpression of *Olfr* genes. *Olfr* gene names are indicated under the X-axis. EV, empty vector as control. (*B*) Relative luciferase signals driven by NF-κB promoter after overexpression of Olfr genes. Mann–Whitney *U* test of mean and SEM (n = 4): *P < 0.05; ***P < 0.001. (*C* and *D*) Western blots of proteins from HEK293T cells transfected with plasmids carrying the indicated Olfr genes. Anti-DDK (*C*) or anti-Olfr1386 antibodies (*D*) were used to detect the Olfr proteins. (*E*) Immunofluorescence Assay (IFA) of Olfr1386 protein localization as described in *Materials and Methods*. Red, anti-DDK antibodies; Green, anti-Olfr1386 antibodies; Blue, DAPI staining the nucleus. (*F*) qPCR measurement of Olfr1386 transcript levels in T-cells, B-cells, dendritic cells (DCs), and macrophages in the spleens before (NI), day 1 (D1), and day 4 (D4) after YM infection. Relative RT-qPCR signals were plotted. Kruskal–Wallis test, n = 6 to 8; *P < 0.05.

The Expression of *Olfr1386* Increases the Phosphorylation of TBK1, IRF3, P38, and JNK. Next, we investigated the cell types expressing *Olfr1386* in vivo and the effects of Olfr1386 on the expression and phosphorylation of some critical molecules in the pathways of IFN-I response, NF-κB signaling, and cell death. We isolated T-cells, B-cells, dendritic cells (DCs), and macrophages from the spleens, performed RT-qPCR to measure Olfr1386 mRNA levels, and showed that only B-cells expressed significantly higher *Olfr1386* mRNA after YM parasite infections, although higher levels (not significant) of *Olfr1386* transcript were also observed in other cell types (Fig. 3*F*). Overexpression of Olfr1386 in HEK293T cells significantly increased the levels of phosphorylated TBK1 (pTBK1), IRF3 (pIRF3), and STAT1 (pSTAT1) but not the protein levels (Fig. 4 *A* and *B*). No change in the protein levels of MAVS, MDA5, RIG-I, STING, STAT2, and pSTAT2 was detected after Olfr1386 overexpression (Fig. 4*C*), suggesting Olfr1386 expression affects TBK1/IRF3 complex downstream of the DNA/RNA sensors. Increased levels of pTBK1 and pIRF3 were also observed in HeLa cells after overexpression of Olfr1386 (*SI Appendix,* Fig. S3*A*). These results show that Olfr1386 can stimulate the phosphorylation of TBK1, IRF3, and STAT1.

GPCRs are known to activate NF-κB (P50/p65) through PKC and IKK (IKKα, β) complex as well as P38 and JNK signaling pathways (P38 and MKK3/6) (43). Overexpression of the Olfr1386 also significantly increased the levels of pP38, P38γ, and pJNK (Fig. 4 *D*–*F*), but not the protein levels of P38, P38α, P38β, P50, P65, pP65, P105, pP105, IKKα, and IKKβ (Fig. 4 *D* and *E* and *SI Appendix,* Fig. S3*B*). The level of pMEKK1/2 was slightly increased in the Olfr1386 transfected cells (Fig. 4*E*), but the increase in pMEK1/2 was not significant. To investigate whether transfection of the cells with the Olfr1386 plasmids caused cell death, we measured the protein levels of CASP3, CASP9, and PARP1 associated with apoptosis. The levels of these proteins were similar in cells not transfected, transfected with the empty vector (EV) or with the Olfr1386 plasmid, and no cleaved CASP3 and CASP9 products were detected either (*SI Appendix,* Fig. S3*C*). These results suggest that, in addition to pTBK1 and pIRF3, the expression of Olfr1386 also activates P38 and JNK pathways (Fig. 4*G*).

Olfr1386 Enhances TLR3-Mediated IFN-I Response with Poly(I:C) Stimulation. Because Olfr1386 has a GPLS pattern similar to that of TLR3 and is reported to be expressed in nonolfactory tissues (21), we also investigated its roles in host immune responses and interaction with TLR3. Again, transfection of HEK293T cells with plasmid encoding Olfr1386 produced luciferase signals driven by the IFN-β promoter significantly higher than those transfected with an empty vector (EV) (Fig. 5*A*). Cotransfection of the HEK239T cells with plasmids containing *Olfr1386* and *Tlr3* genes also generated significantly higher luciferase signals than cells transfected with *Tlr3* and EV with or without poly(I:C) stimulation (Fig. 5*A*). The results suggest potential enhancement of TLR3-mediated IFN-β signal by Olfr1386 after poly(I:C) stimulation. Stimulation of the HEK293T cells with Poly(I:C) did not have a significant effect on the Olfr1386-mediated luciferase signal without TLR3. Similar results were obtained for luciferase signals

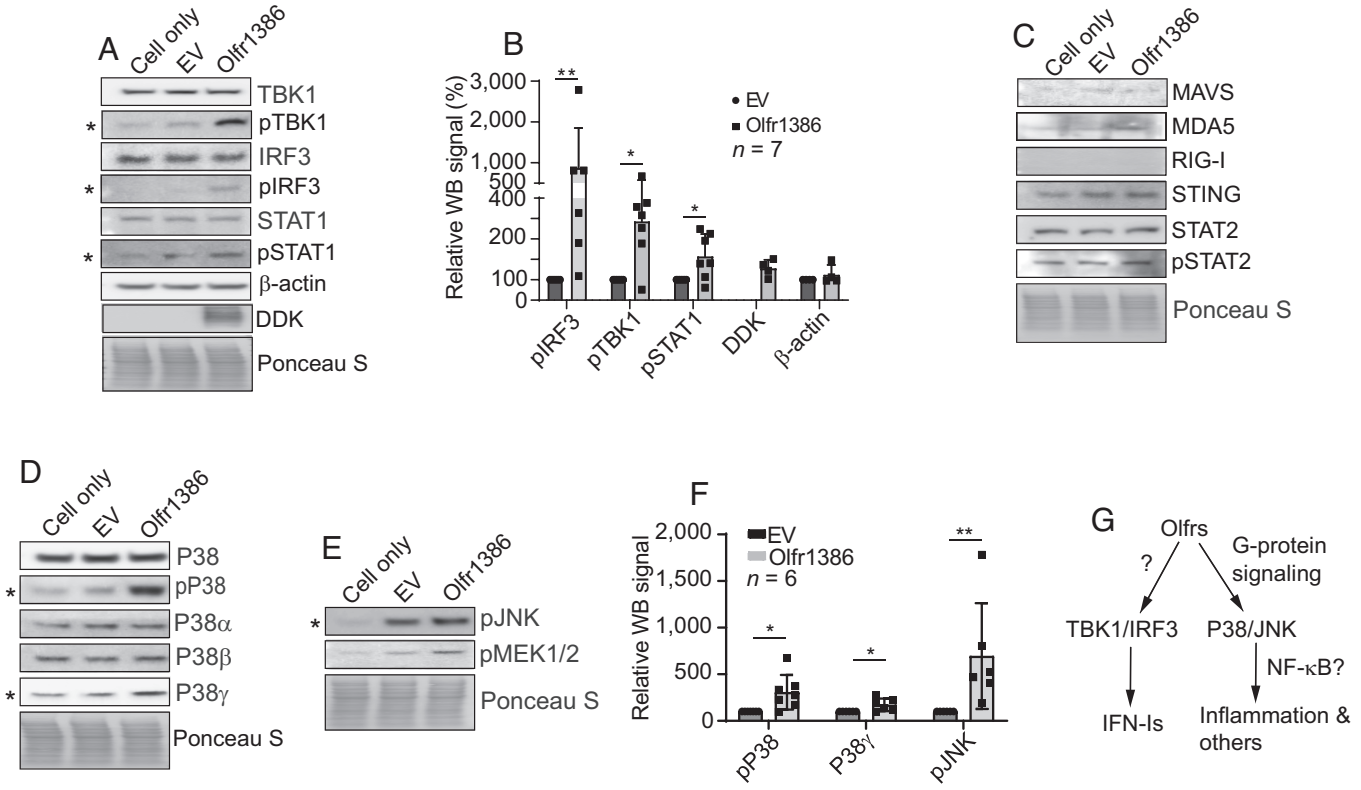

Fig. 4. Western blot detection of expression or phosphorylation of key proteins in immune signaling. (*A*) Western blots of key molecules in IFN-I responses. HEK293T cells were transfected with plasmids (1 μg) carrying the Olfr1386 gene, and cell lysates were run on SDS-PAGE gels 24 h after transfection. EV, empty vector as transfection control; β-actin and/or Ponceau S staining of total proteins as loading controls. All the antibodies obtained from commercial companies are listed in *SI Appendix,* Table S1. Anti-DDK antibodies were used to detect tagged Olfr1386 protein. (*B*) Plots of protein band signals scanned from repeated western blot experiments after adjusting protein loading using Ponceau S-stained signals in (*A*). Mann–Whitney *U* test of mean and SEM ($n = 7$); *$P < 0.05$; **$P < 0.01$. (*C*) The same experiments as in (*A*), except detecting protein expression levels of MAVS, MDA5, RIG-I, STING, STAT2, and pSTAT2. (*D*), The same experiments as in (*A*), except detection of P38, P38 subunits, and phosphorylated P38 (pP38). (*E*) The same experiments as in (*A*), except detection of pJNK and pMEK1/2. (*F*) Plots of signals from western blot detecting pP38, pJNK, and p38γ. Mann–Whitney *U* test of mean and SEM ($n = 6$); *$P < 0.05$; **$P < 0.01$. (*G*) A brief diagram summarizing potential pathways stimulated by the Olfr1386 expression.

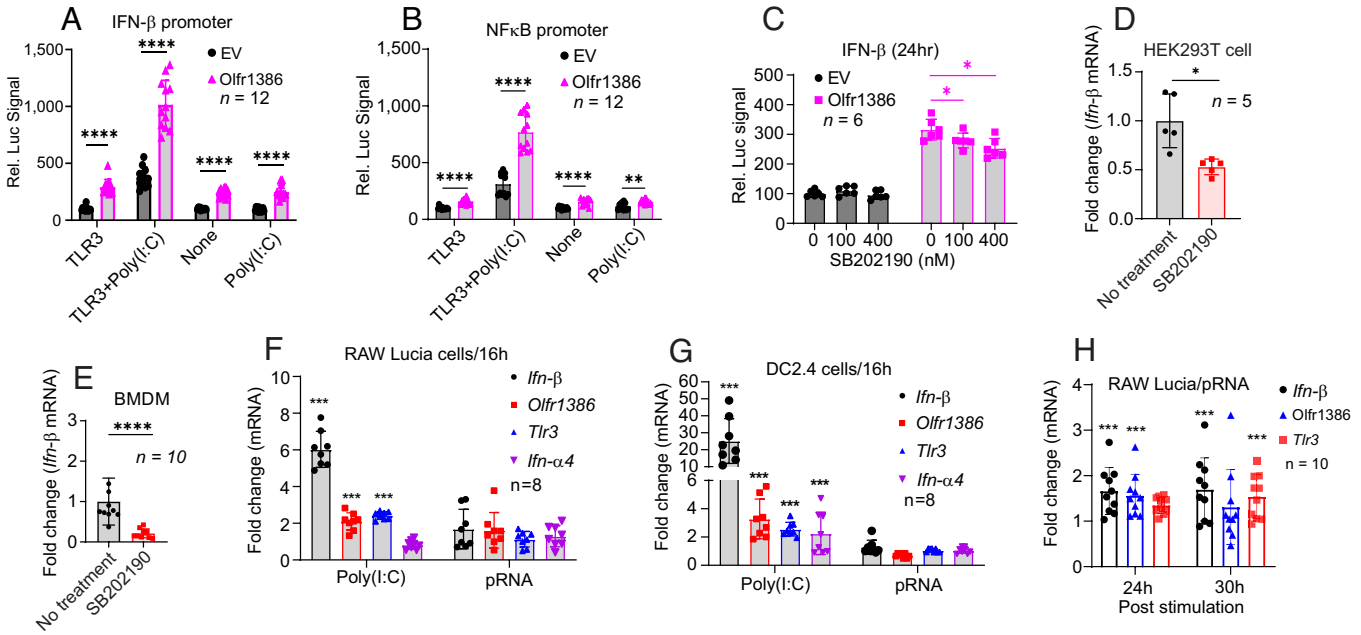

Fig. 5. Interaction of Olfr1386 with TLR3 and P38 pathways as well as stimulation of Olfr1386 expression. (*A* and *B*) HEK293T cells were transfected with plasmids encoding DDK-tagged Olfr1386 (90 ng/each) and/or TLR3 (90 ng/each) as well as firefly (100 ng) and renilla (10 ng) luciferase. Relative (ratio of FLuc/RLuc) luciferase signals were measured 24 h posttransfection and plotted. (*A*) Plots of relative luciferase signals driven by IFN-β promoter after overexpression of Olfr1386 with or without TLR3 and additional poly(I:C) stimulation for 24 h. (*B*) Same as (*A*) with luciferase signals driven by NF-κB promoter. (*C*) Plots of relative luciferase signals with or without SB202190 inhibition of P38 activity at 24 h. EV, empty vector control. (*D*) RT-qPCR measurement of IFN-β mRNA levels after Olfr1386 expression with or without SB202190 (100 nM) treatment of HEK293T cells for 3 h. (*E*) The experiment as in (*D*) except using bone marrow–derived macrophages (BMDM) without Olfr1386 plasmid transfection. (*F* and *G*) RT-qPCR detection of mRNA levels of *Ifn-β, Ifn-α4, Tlr3,* and *Olfr1386* in RAW Lucia and DC2.4 cells after poly(I:C) (5 μg/mL) and parasite RNA (pRNA, 10 μg/mL) stimulations for 16 h, respectively. (*H*) Fold change in *Ifn-β, Olfr1386,* and *Tlr3* mRNA levels in RAW Lucia cells after pRNA stimulation for 24 h or 30 h. Fold changes in mRNA were normalized to those of nonstimulated samples. Mann–Whitney *U* test of mean and SEM (replicates as indicated): $*P < 0.05$; $**P < 0.01$; $***P < 0.001$; $****P < 0.0001$.

driven by NF-κB promoter (Fig. 5*B*). These results show that Olfr1386 can stimulate pathways of IFN-β and NF-κB responses and can also significantly enhance TLR3-mediated IFN-β response with poly(I:C) stimulation.

Inhibition of P38 Activity Decreases IFN-β mRNA Levels. We next investigated the mechanism of IFN-β-induction by Olfr1386 expression. P38α was shown to regulate type III interferon (IFN-λ1) in human monocyte-derived dendritic cells through the RIG-I/MDA5-MAVS-IRF3 pathway (44), and IFN-β mRNA was increased after activation of P38 and JNK signaling pathways (45). Additionally, p38 activity was shown to be essential for viral induction of IFN-I in fibroblasts and DCs (46). We, therefore, investigated the IFN-β level after blocking P38 signaling using inhibitor SB202190. Inhibition of P38 activity in HEK293T cells expressing Olfr1386 significantly reduced the luciferase signal driven by IFN-β promoter 24 h posttransfection (Fig. 5*C*). However, the reduction in IFN-β response was limited after inhibition of the P38 pathway, suggesting the presence of other pathways in stimulating IFN-β.

P38 can also activate MAPK-activated kinase 2 (MK2) to phosphorylate tristetraprolin (TTP) and prevent TTP from promoting IFN-β mRNA degradation (45). We then used RT-qPCR to measure IFN-β mRNA after expression of Olfr1386 in the HEK293T cells with or without SB202190 treatment. SB202119 (100 nM) could significantly reduce IFN-β mRNA levels stimulated by Olfr1386 expression (Fig. 5*D*). Similarly, bone marrow–derived macrophages (BMDM) had significantly decreased IFN-β mRNA after treatment with SB202190 (Fig. 5*E*). Therefore, Olfr1386 signaling can modulate P38 activity which may, in turn, regulate IFN-β mRNA level.

Stimulation of *Olfr1386* and *Tlr3* Expression by Poly(I:C) and Parasite RNA (pRNA). We investigated whether Poly(I:C) and pRNA could stimulate the transcription of *Olfr1386* mRNA. RAW Lucia (a mouse macrophage cell line) cells were incubated with Poly(I:C) and pRNA, and the levels of *Ifn-β, Ifn-α4, Olfr1386,* and *Tlr3* mRNA were measured using RT-qPCR. Compared with those of nonstimulated, significantly higher levels of *Ifn-β, Olfr1386,* and *Tlr3* mRNA, but not *Ifn-α4* mRNA, were detected in RAW Lucia cells 16 h poststimulation with Poly(I:C) (Fig. 5*F*). Similar results, including significantly increased *Ifn-α4* mRNA, were observed in DC2.4 cell line (Fig. 5*G*). Significantly higher levels of *Ifn-β, Olfr1386,* and *Tlr3* mRNA were observed in RAW Lucia cells only after 24 h or 30 h stimulation with pRNA (Fig. 5 *F–H*). These results suggest that ligands such as Poly(I:C) and possibly pRNA can stimulate *Olfr1386, Tlr3,* and *Ifn-β* expression, which may partially explain the similar GPLS curves between *Tlr3* and *Olfr1386*.

Mice without Olfr1386 Produce Lower IFN-α/β after YM Parasite Infection. To better characterize Olfr1386 functions in vivo, we generated *Olfr1386* knockout (KO, *Olfr1386*$^{-/-}$) mice using the CRISPR/Cas9 technique as described previously (47). Two sgRNAs, TAGATTCGTGATCTTTATAG**TGG** and **CCT**GTTCTACCGACCAAGAAATA (reverse orientation), were used to simultaneously cut the 5′ and 3′ UTR regions of the mouse Olfr1386 gene, which resulted in the deletion of the entire coding sequence (*SI Appendix,* Fig. S4*A*). PCR amplification of DNA from CRISPR/Cas9 mutated mice detected several mouse progenies (8229, 9232, and 8233) with a deletion in the Olfr1386 coding region, which resulted in a PCR product of 424 bp instead of the ~1.5 Kb between the two sgRNAs in WT mice (*SI Appendix,* Fig. S4*B*). DNA sequencing of the PCR products confirmed the deletion of the whole Olfr1386 coding sequence with breakpoints within the two sgRNAs (*SI Appendix,* Fig. S4*C*). Homozygous *Olfr1386*$^{-/-}$ were obtained after backcrossing and genotyping mouse offspring.

To investigate the effects of Olfr1386 deletion on the host IFN-I response, we isolated splenocytes from YM-infected WT and Olfr1386$^{-/-}$ mice, incubated the cells with Poly(I:C) for 16 h in vitro, and measured mRNA levels of selected genes in IFN-I response. Significantly lower mRNA levels of *Ifn-b, Ifn-a4, ISG15*, and *Mx1* were observed in the Olfr1386$^{-/-}$ mice than in WT mice (Fig. 6*A*). Similarly, significantly lower levels of IFN-α and IFN-β proteins were detected in the supernatants of Olfr1386$^{-/-}$ splenocyte cultures (1 × 10^7 cells) than in WT cell cultures after Poly(I:C) stimulation (Fig. 6 *B* and *C*). We then injected *P. yoelii* YM-infected RBCs (1 × 10^5) into WT and Olfr1386$^{-/-}$ mice and observed significantly reduced IFN-α and IFN-β in the Olfr1386$^{-/-}$ mice 24 h after infection (Fig. 6 *D* and *E*). Consequently, significantly higher levels of IFN-γ, CCL-2, and CXCL-10, but significantly lower CXCL-1, were observed in the infected Olfr1386$^{-/-}$ mice than in the infected WT mice on day 4 pi (Fig. 6*F*). No significant differences in parasitemia and body weight were observed between the WT and Olfr1386$^{-/-}$ mice after *P. yoelii* YM infections (slightly higher body weight for the Olfr1386$^{-/-}$ mice) (Fig. 6 *G* and *H*). The majority of the Olfr1386$^{-/-}$ mice survived one day longer than WT mice (Fig. 6*I*). These results confirmed an effect of Olfr1386 in IFN-I and other cytokine/chemokine responses during malaria parasite infections and a small effect on host survival.

IFN-I has been shown to play an important role in controlling viral infections. We next transfected HEK293T cells (2.5 × 10^5 seeded) with empty vector (500 ng, negative control) or plasmids containing MAVS (positive control) or Olfr1386 gene and then infected the cells with vesicular stomatitis virus that expresses green fluorescent protein (VSV-GFP, 0.1 MOI) for 16 h. Significant reductions in the percentage of fluorescent cells and mean fluorescence intensity (MFI) were observed between the group transfected with empty vector and groups transfected with the plasmids containing Olfr1386 or MAVS (Fig. 6 *J* and *K*). We also performed similar experiments using dengue and Zika viruses. No significant

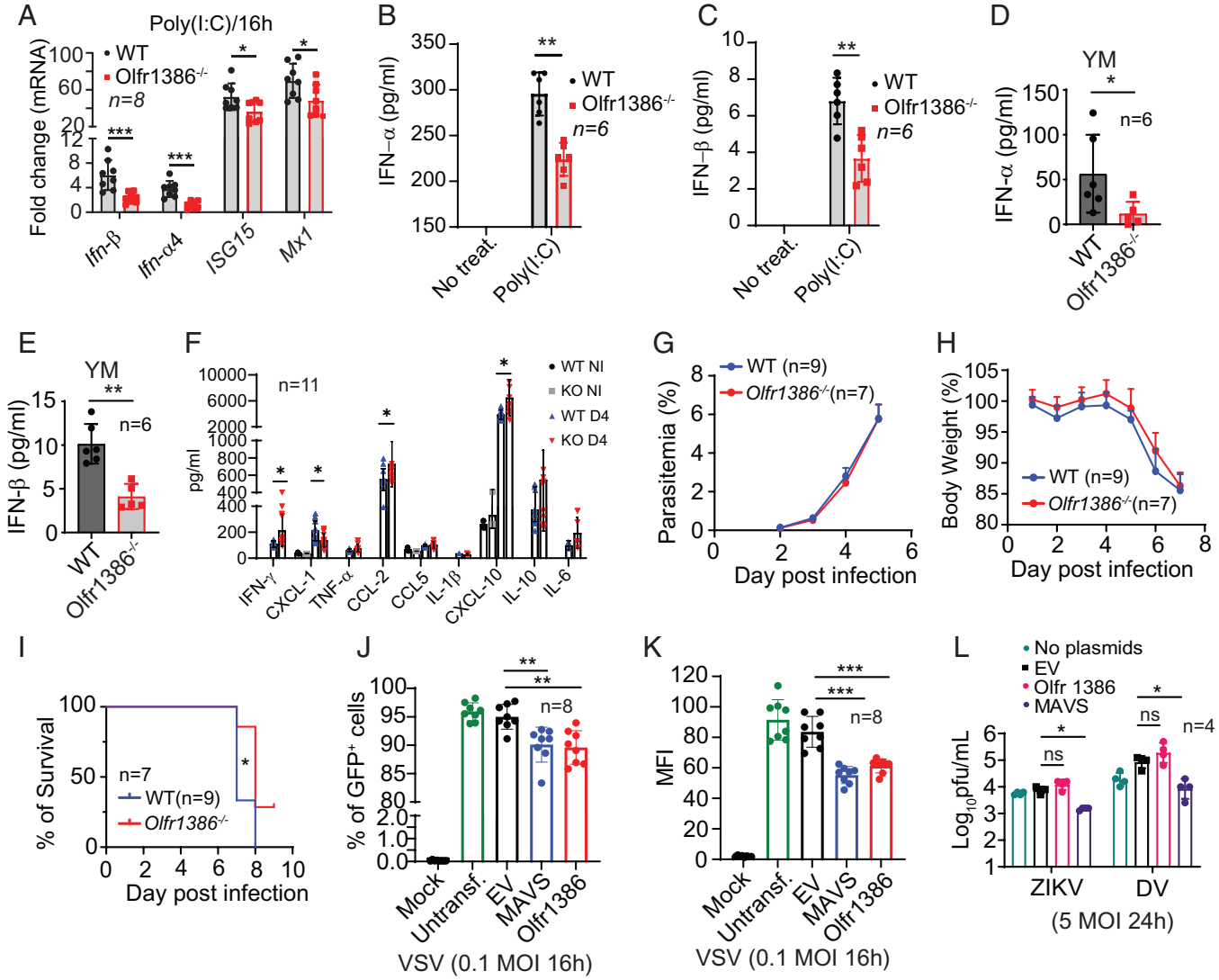

Fig. 6. IFN-I levels and responses to *P. yoelii* infection in WT and Olfr1386$^{-/-}$ mice. (*A*) Fold change in mRNA levels of *Ifn-β, Ifn-α4, ISG15*, and *MX1* in splenocytes (2 × 10^6) from wild-type (WT) and Olfr1386$^{-/-}$ mice 16 h after stimulation with Poly(I:C) (5 μg/mL). (*B* and *C*) IFN-α and IFN-β levels in the supernatants of splenocyte cultures (1 × 10^7) from WT and Olfr1386$^{-/-}$ mice after poly(I:C) (5 μg/mL) stimulation for 16 h. No treat, no treatment. (*D* and *E*) Levels of IFN-α and IFN-β in WT and *Olfr1386*$^{-/-}$ mice 24 h after infection with *P. yoelii* YM parasites. The levels of IFN-α/β in the uninfected mice were under the detection limit of the ELISA. (*F*) Plasma levels of cytokines and chemokines in WT and *Olfr1386*$^{-/-}$ mice day 4 after YM infection. WT NI, noninfected wild-type mice; KO NI, noninfected *Olfr1386*$^{-/-}$ mice; WT D4 and KO D4, wild-type, and *Olfr1386*$^{-/-}$ mice day 4 after YM infection. (*G* and *H*) Parasitemia (*G*), body weight (*H*), and mouse survival time (*I*) after YM infections. (*J* and *K*) HEK293T cells (2.5 × 10^5 seeded) were transfected with empty vector (500 ng) or plasmids containing MAVS or Olfr1386 and infected with vesicular stomatitis virus expressing GFP (VSV-GFP, 0.1 MOI) for 16 h. GFP$^+$ (infected) cells were counted using flow cytometry. (*J*) Plots of the percentage of GFP$^+$ cells from different treatment groups. (*K*) Plots of mean fluorescence intensity (MFI) from the same groups. (*L*) Plots of plaque-forming units after infection with Zika (ZIKV) or dengue (DV) viruses. (*A–F* and *J–K*) Mann–Whitney *U* test of mean and SEM (*n* = 4 to 11): **P* < 0.05; ***P* < 0.01; ****P* < 0.001. For (*I*), Log-Rank test, **P* < 0.05.

differences in plaque-forming unit (PFU) count between the empty vector and Olfr1386 groups were observed, probably due to the rapid growth of the viruses, lower sensitivity of the assay, and/or relatively low levels of IFN-I produced (Fig. 6*L*).

NAD Stimulates Olfr1386 Signaling. To investigate whether the *Olfr1386* gene can be activated by the parasite metabolites, we used a dual-luciferase reporter assay to screen for potential ligands of the *Olfr1386* gene as described previously (48). In this assay, a plasmid containing the Olfr1386 gene was transfected into HEK293T cells along with a firefly luciferase reporter gene construct driven by a cyclic AMP-responsive element (CRE) promoter and a renilla luciferase construct driven by β-actin promoter (*SI Appendix*, Fig. S5*A*). We used 24 potential metabolites previously identified from malaria parasites (49), including nucleosides, amino acids, sugars, and metabolic intermediates (*SI Appendix*, Fig. S5*B*). We also included an EV and forskolin (FKL) as negative and positive controls in the assay, respectively. In the first screen, we pooled all 24 compounds (0.01 to 1.0 mM) as a single ligand mixture in the assay and showed significantly higher luciferase signals driven by CRE promoter from cells expressing *Olfr1386* as well as FKL positive control than that from EV (Fig. 7*A*). We divided the 24 compounds into two groups of 12 each, performed the same assay, and showed that the activities came from the second group of the compounds (Fig. 7*B* and *SI Appendix*, Fig. S5*B*). The second group of 12 compounds was further divided into four subgroups of three compounds each, and the activity was detected from subgroup 4 containing cyclic-di-GMP, NAD, and uridine 5′monophosphate disodium only (Fig. 7*C*). Finally, the activity was confirmed to be from NAD (Fig. 7*D*). The response to NAD was dose-dependent with an estimated half-maximal effective concentration (EC_{50}) value of 18.46 μg/mL (or 27.82 μM) for *Olfr1386* (Fig. 7*E*). These results suggest that increased NAD levels after malaria parasite infections may activate Olfr1386 leading to activation of some specific immune pathways.

Inhibition of G Protein Signaling and Increased IFN-I Responses after NAD Stimulation. The binding of a ligand to the GPCR results in a conformational change of the receptor, leading to activation of the Gα subunit, exchange of GDP to GTP, and

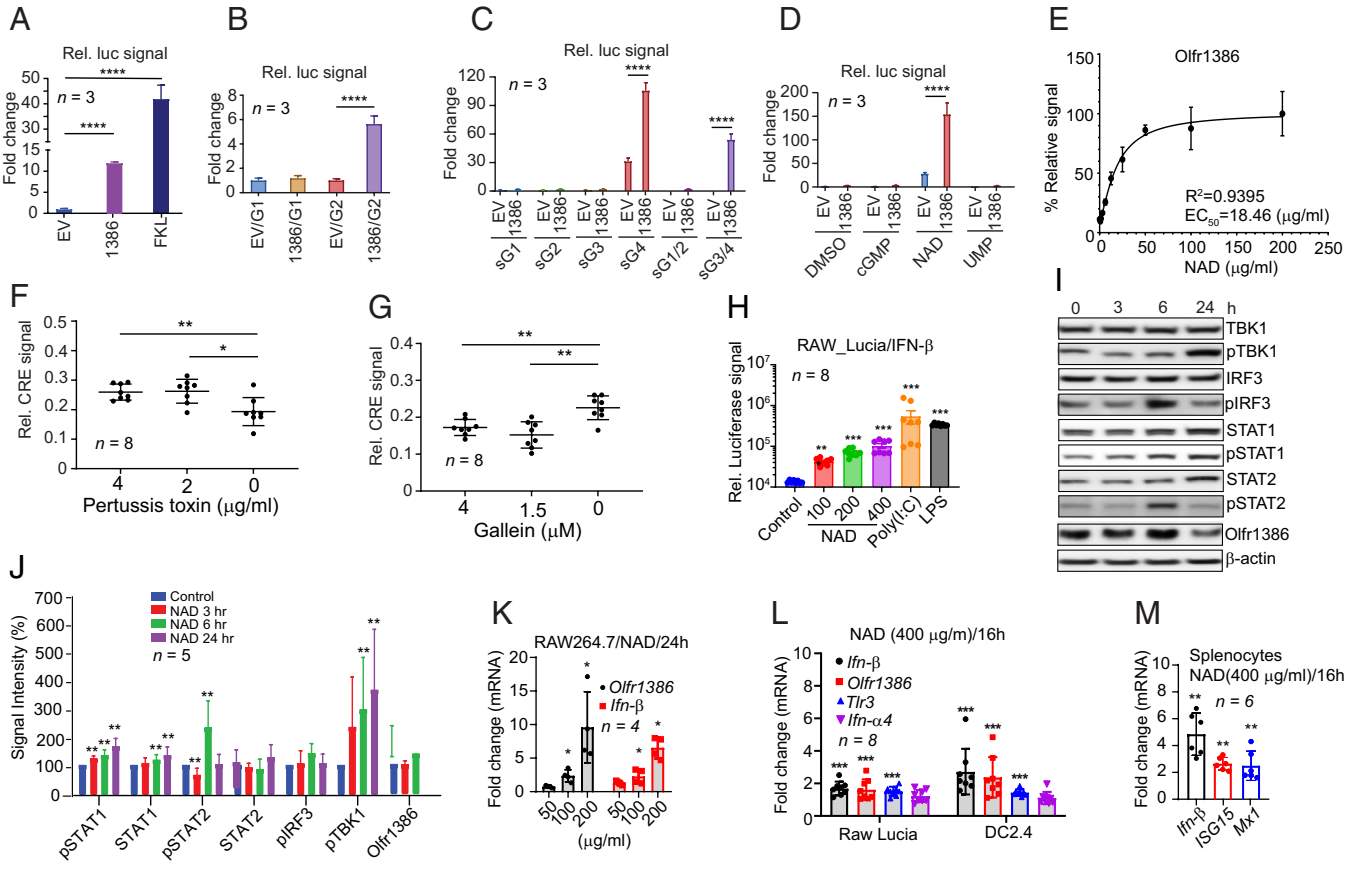

Fig. 7. Screening parasite metabolites for potential Olfr1386 ligand and NAD stimulation of IFN-I responses. A dual-luciferase assay was employed to screen for Olfr-mediated G-protein signaling as described in *Materials and Methods* and *SI Appendix*, Fig. S5*A*. HEK293T cells were transfected with a plasmid containing the *Olfr1386* gene along with a firefly luciferase reporter construct driven by a cyclic AMP-responsive element (CRE) promoter and renilla luciferase construct driven by β-actin promoter. Fold changes in relative signals from firefly adjusted by renilla luciferase signal are plotted. (*A*) Fold changes in relative signals from cells transfected with empty vector (EV, negative control) and a plasmid encoding Olfr1386 after stimulation with a mixture of 24 metabolites (*SI Appendix*, Fig. S5*B*). Forskolin (FKL) was included as a positive control. (*B*) The same experiments as in (*A*), but cells were stimulated with group 1 (G1) or group 2 (G2) each containing 12 metabolites. (*C*) The same experiments as in (*B*), but cells were stimulated with four subgroups (sG1–sG4) of compounds each containing three metabolites. (*D*) Stimulation of cells containing EV or Olfr1386 plasmid with cGMP, NAD, and UMP. For (*B–D*), Two-tailed *t* test of three replicates, ****$P < 0.0001$. (*E*) Dose–response curves and estimates of EC_{50} values after transfection of cells with Olfr1386 plasmid and stimulation with various concentrations of NAD. (*F*) Inhibition of G protein-coupled receptor (GPCR) signaling by pertussis toxin after expression of Olfr1386 in HEK293T cells. (*G*) Inhibition of GPCR signaling by gallein after expression Olfr1386 in HEK293T cells. (*H*) Stimulation of RAW-Lucia cells with NAD (100, 200, and 400 μg/mL, respectively), poly(I:C) (2 μg/mL), and LPS (2 mg/mL). Luciferase signals driven by ISG54 minimal promoter and ISREs were measured after stimulations. (*I*) Western blot of RAW264.7 cell lysates detected using antibodies as indicated 0, 3, 6, and 24 h poststimulation with NAD (200 μg/mL). (*J*) Plots of signals from repeats of experiments in (*I*). (*K*) Plots of relative mRNA levels of Olfr1386 and IFN-β after NAD stimulation of RAW264.7 cells for 24 h. (*L*) Fold change in mRNA levels of *Ifn-β, Ifn-α4, Tlr3,* and *Olfr1386* in RAW Lucia and DC2.4 cells after NAD stimulation for 16 h. (*M*) Fold change in mRNA levels of *Ifn-β, ISG15, and Mx1* after NAD stimulation of splenocytes, compared with nonstimulated cells. For (*F–H* and *J–M*) Mann–Whitney *U* test, mean, and SEM ($n = 4$ to 8): *$P < 0.05$; **$P < 0.01$, ***$P < 0.001$.

dissociation of the Gα subunit from the Gβγ dimer and the receptor. To further confirm that the CRE signal stimulated by NAD was mediated by Olfr1386, we transfected HEK293T cells with a plasmid (90 ng) encoding Olfr1386, stimulated the cells with NAD (100 μg/mL), and inhibited the G protein subunit activities using Gα inhibitor pertussis toxin (PTX) and Gβγ inhibitor gallein, respectively. The results showed that PTX could significantly increase NAD-stimulated CRE signals, while gallein could significantly inhibit NAD-stimulated CRE signals (Fig. 7 *F* and *G*). PTX is known to inhibit Gαi unit that inhibits AC activity (50). Therefore, PTX inhibition of Gαi will increase AC activity, cAMP level, and luciferase signal as observed.

We also treated RAW-Lucia ISG cells (RAW264.7 cell integrated with interferon regulatory factor-inducible Lucia luciferase reporter) with NAD (100 to 400 μg/mL) for 24 h. Dose-dependent and significantly higher luciferase signals were observed 24 h after NAD stimulation, although the signals from NAD treatment were not as high as those from poly(I:C) (2 μg/mL) or lipopolysaccharide (LPS, 2 mg/mL) stimulations (Fig. 7*H*).

Additionally, protein expression and/or phosphorylation of key molecules in IFN-I response pathways including pTBK1 (6 and 24 h), STAT1 (6 and 24 h), pSTAT1 (3, 6, and 24 h), and pSTAT2 (6 h) were significantly increased in RAW264.7 cells after NAD (100 μg/mL) stimulation (Fig. 7 *I* and *J*). pIRF3 was also increased, but the changes were not significant due to variation at different time points (3 h and 6 h) (Fig. 7*I* and *SI Appendix,* Fig. S6). The mRNA levels of *Olfr1386, Tlr3*, and *Ifn-β* were also significantly higher in RAW Lucia and DC2.4 cells after NAD stimulation (Fig. 7 *K* and *L*). Although the protein levels of IFN-α and IFN-β were below the detection limit of a commercial ELISA kit (PBL Assay Science), the higher levels of *ISG15* and *Mx1* mRNAs suggested the production of IFN-I by the splenocytes after NAD stimulation (Fig. 7*M*). These results suggest that NAD can stimulate IFN-I responses as well as increase mRNA levels of *Olfr1386, Tlr3,* and IFN-β in vitro.

Regulated OR Gene Expression in Human Malaria Patients. To further support the observations of Olfr gene responses in rodent malaria, we searched for OR gene expression in multicohort transcriptome studies of whole blood samples published in a recent meta-analysis (51). Data from four different studies comparing gene transcriptions in the whole blood of malaria patients and healthy children were analyzed to show activation of neutrophils, dendritic cells, and type 2 T helper cells (51). Searches of the datasets also detected 42 human OR genes with changed expression in three of the four studies (Dataset S2; One dataset used microarray and detected few genes overall). In particular, samples from the GSE1124 dataset compared gene expression between samples from cerebral, asymptomatic, uncomplicated, and severe patients vs. healthy controls and detected several OR genes with more than twofold changes in expression (Dataset S2). For example, OR1A1 and OR52A1 were expressed at fivefold higher levels in cerebral patients than in the healthy controls. Interestingly, more than 330 human OR genes were detected in both GSE117613 and GSE34404 datasets, including the human homolog gene of Olfr1386 (OR2Y1c) (Dataset S3). The changed expressions of OR genes in human malaria blood samples are consistent with our observations in rodent malaria, suggesting that Olfr/OR genes play a role in host responses to malaria parasite infections.

Discussions

Olfrs are chemoreceptors normally expressed on olfactory sensory neurons in the olfactory epithelium of the nose to detect volatile chemicals (1, 2). However, many Olfrs are expressed outside of the olfactory sensory neurons and have diverse functions in immune responses and disease processes (52, 53). In particular, a recent report showed that human Olfr2 could detect octanal, leading to the activation of the NLR family pyrin domain containing 3 (NLRP3) inflammasome and induction of interleukin-1β secretion in human and mouse macrophages (53). Olfr2 expression in vascular Mϕ was significantly increased after treatment with the TLR4 agonist LPS and was further enhanced in the presence of octanal. Additionally, Olfr2 ligation induced cAMP, Ca^{2+} flux, ROS, inflammasome activation, and IL-1 secretion (53). In another report, an odorant receptor was shown to increase intracellular cAMP to modulate T cell tissue trafficking (54). In *Caenorhabditis elegans*, neuronal GPCR could regulate innate immunity by modulating intestinal p38/MAPK activity (55). In this study, we reveal another important role of Olfrs in regulating IFN-I responses. We show that selected Olfrs identified from genetic analyses of gene expression in mouse spleens infected with *P. yoelii* can modulate phosphorylation levels of several molecules in signaling pathways critical for host immune responses (*SI Appendix,* Fig. S7). Additionally, the majority of the Olfr genes were identified from mouse spleen 24 h pi, but not from those of day 4 pi. These observations suggest that the Olfr genes are expressed outside the olfactory neurons and are activated early during the infections as expected for receptors recognizing parasite or parasite-stimulated ligands. These data are consistent with the detection of a large number of OR genes in the whole blood samples of malaria patients, suggesting the expression of OR genes outside the olfactory sensory neurons in response to malaria parasite infections (51). Because some of the Olfrs such as Olfr1386 and Olfr1373 have GPLSs similar to those of TLR3 and TLR8, respectively, we hypothesized that these Olfrs might play a role in host immunity such as IFN-I responses. Indeed, expression of several Olfrs (Olfr279, 1268, 1317, 1373, and 1386) in HEK293T cells was found to significantly increase the luciferase signals driven by IFN-β and NF-κB promoters, and expression of Olfr1386 in the HEK293T and HeLa cells could also significantly increase the levels of pTBK1, pIRF3, pP38, and pJNK. Further, Olfr1386 could enhance TLR3-mediated IFN-I responses with poly(I:C) stimulation, and poly(I:C) and pRNA could stimulate *Olfr1386* and *Tlr3* transcription. These results are parallel to the observation that Olfr2 expression was increased after treatment with LPS and was further enhanced by octanal (53), revealing potential functional roles of Olfr1386 in regulating host immune responses. Although the molecular mechanisms of how Olfr1386 regulates the phosphorylation of TBK1 and IRF3 require further investigation, our data showed that Olfr1386 could modulate P38 activity that in turn regulated IFN-β mRNA level. These observations support the important role of Olfr1386 in host immunity against malaria infections.

To investigate the functional roles of Olfr1386 in vivo, we deleted the Olfr1386 gene from the mouse genome. The $Olfr1386^{-/-}$ mice produced significantly lower levels of IFN-α/β than the WT mice after *P. yoelii* YM infections, which supports the ex vivo observations of increased IFN-I responses after Olfr1386 overexpression in HEK293T and HeLa cells. Additionally, small differences in host body weight and survival time were observed between WT and $Olfr1386^{-/-}$ mice after YM infections. The results suggest that although Olfr1386 can contribute to host immune responses, it is not a major molecule that can dominate the direction of host immune responses and survival. Other copies of the Olfr gene family may compensate for the functions in the absence of *Olfr1386*. In our previous studies using *P. yoelii* N67 infection, increased early (24 h) IFN-I levels could suppress parasitemia (56). In this study, $Olfr1386^{-/-}$ mice

with lower IFN-I levels appeared to survive longer than the WT mice. However, parasitemia and host survival time are two different phenotypes. In another study, *P. yoelii* N67- or YM-infected *March1*$^{-/-}$ mice also had significantly reduced serum IFN-I levels day 1 pi and survived longer than WT mice due to elevated levels of IFN-γand CD86^{+} DCs (47). Further, detrimental effects of IFN-I in other rodent malaria models have also been reported previously (57). More studies using different parasite species or strains will help explain the differences.

NAD is identified as a potential ligand for Olfr1386. Olfr1386-mediated signaling could be activated by NAD in a dose-dependent manner, but not by the other 23 malarial metabolites tested, suggesting that the NAD-induced signal is not from background noise. The luciferase signals induced by NAD could also be modulated by compounds (PTX and gallein) that inhibit G protein subunits. NAD treatment of RAW-Lucia or RAW264.7 cells significantly increased IFN-I responses and phosphorylation levels of TBK1 and STAT1/2, suggesting activation of IFN-I pathways. Additionally, the Olfr1386$^{-/-}$ mice produced significantly lower levels of IFN-α/β 24 h after *P. yoelii* YM infection, but had significantly higher levels of IFN-γ, CCL-2, and CXCL-10 on day 4 pi. These changes in cytokine and chemokine levels could affect the activation and migration of T cells, macrophages, and other immune cells. Our observations suggest that NAD can regulate innate immunity through Olfr1386 signaling and P38 activation, which may in turn activate MAPK-activated kinase 2 (MK2) to phosphorylate tristetraprolin (TTP) and prevent TTP from promoting IFN-β mRNA degradation. Increased day-4 levels of IL-10 and IFN-γ with a better host survival rate but reduced levels of IFN-α/β 24 h pi were also observed in *March1*$^{-/-}$ mice after YM infection (42), which suggests a common immune protective mechanism.

The Olfr1386 protein has a "DRY" amino acid motif (*SI Appendix*, Fig. S2*B*) belonging to GPCR family A that includes rhodopsin and the β2-adrenergic receptors (58). Members in this family can bind epinephrine, norepinephrine, serotonin, dopamine, histamine, adenosine, nucleotides, etc. (58). Therefore, Olfr1386 has a structure potential for binding NAD. *Plasmodium falciparum*-infected erythrocytes have been shown to have approximately 10 times higher NAD levels compared to uninfected erythrocytes (59). The parasites cannot synthesize NAD de novo, and the elevated NAD levels might aid *P. falciparum* in establishing infection (60). NAD modulation induces premature eryptosis in human erythrocytes during *P. falciparum* parasite infections (61). Whether changes in NAD level during malaria parasite infections can activate Olfr1386 signaling in vivo to regulate host immune responses require further investigations. We do not know the dynamics of NAD concentrations in the blood or specific organs during malaria parasite infections. Additionally, the investigation of gene families with multiple members, such as the Olfrs, is complicated by potential functional compensation (after depletion of a gene), and more than one paralogous protein may be targeted by an inhibitor or a stimulating ligand. We cannot rule out that NAD may activate additional Olfrs which may compensate for the defect in Olfr1386 function.

The observation of similar GPLSs for *Tlr3* and *Olfr1386* is interesting and intriguing, which is likely due to the similar mRNA expression dynamics of the two genes in mice after infection with the progenies of the N67 × 17XNL cross. Because poly(I:C), NAD, or pRNA stimulation could increase the mRNA levels of both *Tlr3* and *Olfr1386* in cell lines simultaneously, it is possible that pRNA, NAD, and/or other unknown parasite ligands can stimulate *Tlr3* and *Olfr1386* mRNA expression in vivo by the same or a common mechanism. The mouse *Tlr3* and Olfr1386 genes are located on chromosomes 8 and 11, respectively, which rules out the possibility of "cotranscription" by a single promoter. Additionally, the expression of Tlr3 or Olfr1386 could also increase levels of pTBK1 and pIRF1, suggesting potential coregulation of the TBK1/IRF3 pathway by TLR3 or Olfr1386. Indeed, HEK293T cells coexpressing TLR3 and Olfr1386 produced significantly higher levels of IFN-β signal than cells expressing TLR3 alone. However, we cannot rule out that the observed higher IFN-β signal was due to increased IFN-β mRNA level after activation of the Olfr1386-MK2-P38-TTP pathway. The mechanisms of how Olfr1386 expression increases the levels of pTBK1 and pIRF3 and how Olfr1386 regulates TLR3-mediated response, or vice versa, require further investigation.

We recognize the limits of our current study, not being able to thoroughly characterize the function of the Olfr1386 or other Olfrs in vivo during malaria parasite infections because of being a member of a large gene family. Potential experiments to be performed in the future include tagging Olfr1386 with HA or DDK tag that will allow expressional evaluation of Olfr1386 protein in specific tissues or cell populations during malaria parasite infections. Nonetheless, our study demonstrates that some Olfrs, including Olfr1386, can respond to malaria parasite infections, particularly regulating IFN-I responses through changes in gene transcription and protein activity by parasite ligands.

Materials and Methods

Infection of Mice and Ethics Statement. Infection of mice with *P. yoelii* YM parasites was reported previously (41, 62). The animal procedures for this study were performed following the protocol approved (approval #LMVR11E) by the Institutional Animal Care and Use Committee at the National Institute of Allergy and Infectious Diseases (NIAID) following the guidelines of the Public Health Service Policy on Humane Care and Use of Laboratory Animals and AAALAC. All mice were maintained under specific pathogen-free conditions.

Cell Culture and Transfection. HEK293T, HeLa, RAW264.7, and RAW-Lucia cells as well as BMDM were cultured in DMEM (Gibco Laboratories, MD) supplemented with 10% fetal bovine serum and antibiotic-antimycotic (Gibco) plus 10% supernatant of L929 M-CSF cells at 37 °C and 5% CO_2 atmosphere. For transfection, cells were plated on a 24-well plate, grown to 50 to 70% confluency, and transfected with plasmid DNA using Lipofectamine 3000 Reagent (Invitrogen) unless stated otherwise. Cells were cotransfected with firefly and renilla luciferase reporter plasmids and individual Olfr plasmids. The total amount of transfected DNA was kept constant in all groups by adding a parental pCMV6 plasmid. After 24 h, cells were washed with phosphate-buffered saline (PBS) and lysed with Passive Lysis Buffer (Promega). Luciferase reporter activity was assessed using the Dual-Luciferase Reporter Assay (Promega), and luminescence intensity was measured using a Microplate Reader (GloMax Discover Explore System, Promega).

Ligand Screening. The HEK293T cells on 96-well plates were cotransfected with 100 ng IFN-β or NF-κB_FL reporter plasmids, 90 ng Olfr plasmids, and 10 ng β-actin_RL reporter plasmid. The mixtures of ligands (metabolites) were prepared in culture media and added into each well in triplicates. After 4 to 6 h of incubation at 37 °C and 5% CO_2 atmosphere, the culture medium was removed from the plate, and the cells were lysed using Passive Lysis Buffer (Promega). The ligand–receptor response was measured as luminescence of firefly and renilla reporters in a cell-based assay following the protocol for the Dual-Glo Luciferase Assay System (Promega).

Generation of Olfr1386 Knockout Mice. The Orlf1386 knockout mouse line was generated using the CRISPR/Cas9 method (47). Additional Methods can be found in *SI Appendix*.

Data, Materials, and Software Availability. All study data are included in the article and/or supporting information.

ACKNOWLEDGMENTS. This work was supported by the Division of Intramural Research, National Institute of Allergy and Infectious Diseases (NIAID) and the Intramural Research Programs of the National Center for Advancing Translational Sciences, NIH, USA, and in part by the NSF of Human Province (2022RC1069 and 2021SK1010) to L.X. We also thank Yolanda L. Jones, NIH Library Editing Service, for manuscript editing assistance.

Author affiliations: [a]Laboratory of Malaria and Vector Research, National Institute of Allergy and Infectious Disease, NIH, Rockville, MD 20852; [b]RNA Viruses Section, Laboratory of Infectious Diseases, National Institute of Allergy and Infectious Diseases, NIH, Bethesda, MD 20892; [c]Hunan Key Laboratory of Medical Genetics, Key Lab of Rare Pediatric Disease of Ministry of Education, School of Life Sciences, Central South University, Changsha, Hunan 410083, People's Republic of China; [d]Biological Imaging Section, National Institute of Allergy and Infectious Diseases, NIH, Bethesda, MD 20892; [e]National Center for Advancing Translational Sciences, NIH, Bethesda, MD 20892; and [f]Transgenic Core Facility, National Heart, Lung, and Blood Institute, NIH, Bethesda, MD 20892

1. B. Kobilka, G. F. Schertler, New G-protein-coupled receptor crystal structures: Insights and limitations. *Trends Pharmacol. Sci.* **29**, 79–83 (2008).
2. D. M. Rosenbaum, S. G. Rasmussen, B. K. Kobilka, The structure and function of G-protein-coupled receptors. *Nature* **459**, 356–363 (2009).
3. S. T. Wong *et al.*, Disruption of the type III adenylyl cyclase gene leads to peripheral and behavioral anosmia in transgenic mice. *Neuron* **27**, 487–497 (2000).
4. J. Zheng, W. N. Zagotta, Stoichiometry and assembly of olfactory cyclic nucleotide-gated channels. *Neuron* **42**, 411–421 (2004).
5. A. B. Stephan *et al.*, ANO2 is the cilial calcium-activated chloride channel that may mediate olfactory amplification. *Proc. Natl. Acad. Sci. U.S.A.* **106**, 11776–11781 (2009).
6. B. C. Schroeder, T. Cheng, Y. N. Jan, L. Y. Jan, Expression cloning of TMEM16A as a calcium-activated chloride channel subunit. *Cell* **134**, 1019–1029 (2008).
7. Y. D. Yang *et al.*, TMEM16A confers receptor-activated calcium-dependent chloride conductance. *Nature* **455**, 1210–1215 (2008).
8. L. J. Brunet, G. H. Gold, J. Ngai, General anosmia caused by a targeted disruption of the mouse olfactory cyclic nucleotide-gated cation channel. *Neuron* **17**, 681–693 (1996).
9. L. Belluscio, G. H. Gold, A. Nemes, R. Axel, Mice deficient in G(olf) are anosmic. *Neuron* **20**, 69–81 (1998).
10. G. Glusman, I. Yanai, I. Rubin, D. Lancet, The complete human olfactory subgenome. *Genome Res.* **11**, 685–702 (2001).
11. S. Zozulya, F. Echeverri, T. Nguyen, The human olfactory receptor repertoire. *Genome Biol.* **2**, RESEARCH0018 (2001).
12. Y. Niimura, M. Nei, Evolution of olfactory receptor genes in the human genome. *Proc. Natl. Acad. Sci. U.S.A.* **100**, 12235–12240 (2003).
13. X. Zhang, S. Firestein, The olfactory receptor gene superfamily of the mouse. *Nat. Neurosci.* **5**, 124–133 (2002).
14. J. M. Young *et al.*, Different evolutionary processes shaped the mouse and human olfactory receptor gene families. *Hum. Mol. Genet* **11**, 535–546 (2002).
15. Y. Niimura, M. Nei, Comparative evolutionary analysis of olfactory receptor gene clusters between humans and mice. *Gene* **346**, 13–21 (2005).
16. Z. Chen, H. Zhao, N. Fu, L. Chen, The diversified function and potential therapy of ectopic olfactory receptors in non-olfactory tissues. *J. Cell Physiol.* **233**, 2104–2115 (2018).
17. T. Tong, Y. Wang, S. G. Kang, K. Huang, Ectopic odorant receptor responding to flavor compounds: Versatile roles in health and disease. *Pharmaceutics* **13**, 1314 (2021).
18. F. Gaudel *et al.*, Expression of the cerebral olfactory receptors Olfr110/111 and Olfr544 is altered during aging and in Alzheimer's disease-like mice. *Mol. Neurobiol.* **56**, 2057–2072 (2019).
19. S. Conzelmann *et al.*, A novel brain receptor is expressed in a distinct population of olfactory sensory neurons. *Eur. J. Neurosci.* **12**, 3926–3934 (2000).
20. C. Wu *et al.*, Olfactory receptor 544 reduces adiposity by steering fuel preference toward fats. *J. Clin. Invest.* **127**, 4118–4123 (2017).
21. N. Kang *et al.*, Olfactory receptor Olfr544 responding to azelaic acid regulates glucagon secretion in alpha-cells of mouse pancreatic islets. *Biochem. Biophys. Res. Commun.* **460**, 616–621 (2015).
22. S. Itakura, K. Ohno, T. Ueki, K. Sato, N. Kanayama, Expression of Golf in the rat placenta: Possible implication in olfactory receptor transduction. *Placenta* **27**, 103–108 (2006).
23. M. Parmentier *et al.*, Expression of members of the putative olfactory receptor gene family in mammalian germ cells. *Nature* **355**, 453–455 (1992).
24. L. L. Xu *et al.*, Quantitative expression profile of PSGR in prostate cancer. *Prostate Cancer Prostatic Dis.* **9**, 56–61 (2006).
25. L. L. Xu *et al.*, PSGR, a novel prostate-specific gene with homology to a G protein-coupled receptor, is overexpressed in prostate cancer. *Cancer Res.* **60**, 6568–6572 (2000).
26. J. Weng *et al.*, PSGR2, a novel G-protein coupled receptor, is overexpressed in human prostate cancer. *Int. J. Cancer* **118**, 1471–1480 (2006).
27. T. Cui *et al.*, Olfactory receptor 51E1 protein as a potential novel tissue biomarker for small intestine neuroendocrine carcinomas. *Eur. J. Endocrinol.* **168**, 253–261 (2013).
28. D. Massberg *et al.*, Monoterpene (-)-citronellal affects hepatocarcinoma cell signaling via an olfactory receptor. *Arch Biochem. Biophys.* **566**, 100–109 (2015).
29. B. Kalbe *et al.*, Helional-induced activation of human olfactory receptor 2J3 promotes apoptosis and inhibits proliferation in a non-small-cell lung cancer cell line. *Eur. J. Cell Biol.* **96**, 34–46 (2017).
30. M. Chen, R. R. Reed, A. P. Lane, Acute inflammation regulates neuroregeneration through the NF-kappaB pathway in olfactory epithelium. *Proc. Natl. Acad. Sci. U.S.A.* **114**, 8089–8094 (2017).
31. M. Chen, R. R. Reed, A. P. Lane, Chronic inflammation directs an olfactory stem cell functional switch from neuroregeneration to immune defense. *Cell Stem Cell* **25**, 501–513.e505 (2019).
32. K. Kotlo *et al.*, The olfactory G protein-coupled receptor (Olfr-78/OR51E2) modulates the intestinal response to colitis. *Am. J. Physiol. Cell Physiol.* **318**, C502–C513 (2020).
33. R. J. Lee *et al.*, T2R38 taste receptor polymorphisms underlie susceptibility to upper respiratory infection. *J. Clin. Invest.* **122**, 4145–4159 (2012).
34. H. P. Barham *et al.*, Association between bitter taste receptor phenotype and clinical outcomes among patients with COVID-19. *JAMA Netw. Open* **4**, e2111410 (2021).
35. V. C. de Jesus, M. Singh, R. J. Schroth, P. Chelikani, C. A. Hitchon, Association of bitter taste receptor T2R38 polymorphisms, oral microbiota, and rheumatoid arthritis. *Curr. Issues Mol. Biol.* **43**, 1460–1472 (2021).
36. H. O. Smail, The roles of genes in the bitter taste. *AIMS Genet.* **6**, 88–97 (2019).
37. J. Meijerink, M. A. Braks, J. J. Van Loon, Olfactory receptors on the antennae of the malaria mosquito Anopheles gambiae are sensitive to ammonia and other sweat-borne components. *J. Insect Physiol.* **47**, 455–464 (2001).
38. I. V. Coutinho-Abreu, J. A. Riffell, O. S. Akbari, Human attractive cues and mosquito host-seeking behavior. *Trends Parasitol.* **38**, 246–264 (2021), 10.1016/j.pt.2021.09.012.
39. Y. T. Qiu, J. J. van Loon, W. Takken, J. Meijerink, H. M. Smid, Olfactory coding in antennal neurons of the malaria mosquito. *Anopheles gambiae. Chem. Senses* **31**, 845–863 (2006).
40. M. Kelly *et al.*, Malaria parasites produce volatile mosquito attractants. *mBio* **6**, e00235-15 (2015).
41. J. Wu *et al.*, Genome-wide Analysis of Host–*Plasmodium yoelii* Interactions Reveals Regulators of the Type I Interferon Response. *Cell Rep.* **12**, 661–672 (2015).
42. J. Wu *et al.*, The E3 ubiquitin ligase MARCH1 regulates antimalaria immunity through interferon signaling and T cell activation. *Proc. Natl. Acad. Sci. U.S.A.* **117**, 16567–16578 (2020).
43. V. Wu *et al.*, Illuminating the Onco-GPCRome: Novel G protein-coupled receptor-driven oncocrine networks and targets for cancer immunotherapy. *J. Biol. Chem.* **294**, 11062–11086 (2019).
44. M. Jiang *et al.*, MAP kinase p38alpha regulates type III interferon (IFN-lambda1) gene expression in human monocyte-derived dendritic cells in response to RNA stimulation. *J. Leukoc Biol.* **97**, 307–320 (2015).
45. V. A. McGuire *et al.*, Beta interferon production is regulated by p38 mitogen-activated protein kinase in macrophages via both MSK1/2- and tristetraprolin-dependent pathways. *Mol. Cell Biol.* **37**, e00454-16 (2017).
46. S. S. Mikkelsen *et al.*, RIG-I-mediated activation of p38 MAPK is essential for viral induction of interferon and activation of dendritic cells: Dependence on TRAF2 and TAK1. *J. Biol. Chem.* **284**, 10774–10782 (2009).
47. X. He *et al.*, RTP4 inhibits IFN-I response and enhances experimental cerebral malaria and neuropathology. *Proc. Natl. Acad. Sci. U.S.A.* **117**, 19465–19474 (2020).
48. H. Zhuang, H. Matsunami, Evaluating cell-surface expression and measuring activation of mammalian odorant receptors in heterologous cells. *Nat. Protoc.* **3**, 1402–1413 (2008).
49. K. L. Olszewski *et al.*, Host-parasite interactions revealed by *Plasmodium falciparum* metabolomics. *Cell Host Microbe* **5**, 191–199 (2009).
50. C. Locht, L. Coutte, N. Mielcarek, The ins and outs of pertussis toxin. *FEBS J.* **278**, 4668–4682 (2011).
51. Y. H. Zhang, X. Z. Su, J. Li, J. J. Shi, L. H. Xie, Multicohort transcriptome analysis of whole blood identifies robust human response signatures in *Plasmodium falciparum* infections. *Malar J.* **21**, 333 (2022).
52. D. Massberg, H. Hatt, Human olfactory receptors: Novel cellular functions outside of the nose. *Physiol. Rev.* **98**, 1739–1763 (2018).
53. M. Orecchioni *et al.*, Olfactory receptor 2 in vascular macrophages drives atherosclerosis by NLRP3-dependent IL-1 production. *Science* **375**, 214–221 (2022).
54. A. A. Clark, S. Nurmukhambetova, X. Li, S. D. Munger, J. R. Lees, Odorants specifically modulate chemotaxis and tissue retention of CD4+ T cells via cyclic adenosine monophosphate induction. *J. Leukoc Biol.* **100**, 699–709 (2016).
55. S. R. Venkatesh, V. Singh, G protein-coupled receptors: The choreographers of innate immunity in *Caenorhabditis elegans*. *PLoS Pathog.* **17**, e1009151 (2021).
56. J. Wu *et al.*, Strain-specific innate immune signaling pathways determine malaria parasitemia dynamics and host mortality. *Proc. Natl. Acad. Sci. U.S.A.* **111**, E511–E520 (2014).
57. I. Sebina *et al.*, IFNAR1-signalling obstructs ICOS-mediated humoral immunity during non-lethal blood-stage plasmodium infection. *PLoS Pathog.* **12**, e1005999 (2016).
58. G. E. Rovati, V. Capra, R. R. Neubig, The highly conserved DRY motif of class A G protein-coupled receptors: Beyond the ground state. *Mol. Pharmacol.* **71**, 959–964 (2007).
59. C. R. Zerez, E. F. Roth Jr., S. Schulman, K. R. Tanaka, Increased nicotinamide adenine dinucleotide content and synthesis in *Plasmodium falciparum*-infected human erythrocytes. *Blood* **75**, 1705–1710 (1990).
60. J. K. O'Hara *et al.*, Targeting NAD+ metabolism in the human malaria parasite *Plasmodium falciparum*. *PLoS One* **9**, e94061 (2014).
61. A. Chaurasiya *et al.*, Pathogen induced subversion of NAD(+) metabolism mediating host cell death: A target for development of chemotherapeutics. *Cell Death Discov.* **7**, 10 (2021).
62. J. Li *et al.*, Linkage maps from multiple genetic crosses and loci linked to growth-related virulent phenotype in *Plasmodium yoelii*. *Proc. Natl. Acad. Sci. U.S.A.* **108**, E374–E382 (2011).